IEEE Access
Multidisciplinary | Rapid Review | Open Access Journal

Received April 30, 2022, accepted May 16, 2022, date of publication May 18, 2022, date of current version May 25, 2022.

Digital Object Identifier 10.1109/ACCESS.2022.3176364

Design and Research of a Dual Rotor Consequent-Pole Vernier Motor With Halbach Array

YING XIE, (Senior Member, IEEE), SHOUCONG HE, JIAWEI SHAO, BITIAN YE, FAN YANG, AND LIJING WANG

Electrical and Electronic Engineering Department, Harbin University of Science and Technology, Harbin 150080, China

Corresponding author: Ying Xie (xieying_1975@163.com)

This work was supported by the National Natural Science Foundation of China under Grant 51977052 and Grant U21A20145.

ABSTRACT Aiming at improving the torque density of the motor and the utilization rate of permanent magnets (PMs), a dual rotor consequent-pole vernier motor (DRCPVM) is proposed in this article. The stator of the motor has a double-sided structure with two sets of independent windings on each side. Therefore, the proposed motor has different working modes according to the on/off state of the two sets of windings. In the design process, DRCPVM is used as a basic model and optimization is performed on it. The optimization includes the slot width and height of the stator teeth and the radian ratio occupied by the PMs. Moreover, the Halbach array is introduced into the consequent-pole structure to establish the dual rotor consequent-pole vernier motor with Halbach array (DRCPVM-HA). Halbach array reduces flux leakage and improves the magnetic circuit. And Halbach array is employed to discuss the design of the magnetization angle. The rule of the electromagnetic performance changing with the magnetization angle is studied to find the optimal magnetization angle in the Halbach array. When the magnetization angle is 45° in DRCPVM-HA, the torque is significantly improved, the torque ripple is reduced, and the utilization rate of PMs is improved.

INDEX TERMS Vernier motor, outer rotor, inner rotor, magnetization angle, Halbach array.

I. INTRODUCTION

Permanent magnet motors have been developed rapidly in the last several years because of their compact structure and efficient performance. Due to the demand for low-speed and high torque density motors, the volume of conventional permanent magnet synchronous motors (PMSM) is large, and the torque density is difficult to meet the requirement. Based on magnetic field modulation, novel permanent magnet vernier motors (PMVM) have been proposed and have attracted considerable attention. Novel control systems can be also used to optimize motor performance. To improve the speed regulation system of PMSM, a novel control strategy is proposed in [1], which includes the combination of disturbance observer and algorithm. A generalized proportional integral observer is adopted and combined with control methods to avoid dynamic disturbances [2].

Meanwhile, various new vernier motor structures have been proposed by experts and scholars. By comparison with the same volume motors, vernier motors have higher torque and smooth no-load EMF waveform [3]. Introducing DC field windings based on the original vernier motor structure to realize the magnetic flux control [4]. The DC field windings play an important role in enhancing excitation to improve the power factor. And the DC field windings between the stator teeth, take advantage of the characteristics of the consequent-pole structure to realize weak magnetic control [5].

Besides, various structures are proposed for the vernier motors to have better electromagnetic performance, such as dual stator and dual rotor. The double stator structure can meet the demand for increasing torque density, and independent windings make the motor have flexible control strategies [6]. Establishing the equivalent model and analytical calculation is performed in a dual stator structure [7]. To reduce the copper loss and increase torque, a dual-rotor structure with toroidal winding is proposed in [8]. In the vernier motors, the air-gap magnetic flux is crucial. Vernier motor makes more use of harmonic components in the air gap and performs better than the flux-reversal motor [9].

The associate editor coordinating the review of this manuscript and approving it for publication was Shihong Ding.

Other order air-gap harmonics are introduced by adopting the structure of the unequal tooth pitch, which has an increase in torque density [10]. For the same size motors, using the method of placing PMs on both sides of the stator and rotor is to increase torque and induced voltage. Slots of stator and rotor have PMs, both sides play the role of modulation through their teeth structure [11], [12]. The different placement positions of PMs are compared, and it is found that the rotor-PMs motor has better performance. For dual permanent magnet structure, PMs on the rotor have higher utilization than those on the stator, and the parameters are established on the rotor in priority [13], [14]. To improve torque and reduce torque ripple, optimization strategies for permanent magnets are proposed, which include the Halbach array. Fault-tolerant structure with five phases is proposed, which has a higher torque density. By analyzing the original and Halbach array structure, the results show that the Halbach array improves the electromagnetic performance of the motor [15], [16]. Part of the original PMs of the rotor is placed in the stator slots, and the Halbach array is introduced into them. Both the no-load back-EMF and the torque of the motor are improved [17]. Meanwhile, use fewer magnets in the consequent-pole structure than those in the traditional structure, and obtain better performance with optimization. In the consequent-pole motor, the volume of PMs is reduced and the cost of the motor is also reduced [18], [19]. But the consequent-pole structure will cause magnetic flux leakage [20]. The consequent poles with the Halbach array will reduce the magnetic flux leakage, and the Halbach array is also introduced to improve the no-load back-EMF and trust density [21]. With the development of vernier motors, various topologies have been applied to specific requirements such as torque and power density. The dual-rotor structure is an effective way to improve the motor torque density without changing its volume. However, due to the dual-rotor structure, the consumption of permanent magnets is high. In the case of little change in motor performance, the amount of PMs can be decreased by consequent poles. Through the cooperation of consequent poles structure and Halbach array, the performance of the motor can be further improved.

In this article, a novel dual-rotor consequent-pole vernier motor is proposed, and research has been carried out. The dual-rotor structure utilizes the internal space of the motor itself to enhance the overall torque output capacity. Meanwhile, the consumption of PMs can be reduced by introducing consequent poles. For performance improvement, the Halbach array is introduced into the structure when the consequent pole is adopted, and the structural parameters of the motor are optimized at the same time. The law that changes in electromagnetic performance with the magnetization angle of the Halbach array is also verified by the FEA. By comparison, the electromagnetic characteristics of two kinds of motor models are analyzed.

The article is organized as follows. Section II gives the topologies of the motors, and introduces the operating principle of vernier motors. In Section III, the optimization strategies are mainly discussed, and motor parameters have been determined. In Section IV, the performance of the motors is compared and analyzed. Brief conclusions are given in Section V.

The main contributions of this paper are summarized as follows. Firstly, the dual-rotor motor structure is proposed to improve the torque density, and the consequent-pole structure is used to reduce the amount of PMs. Secondly, the optimization strategy of the proposed motor is given. Thirdly, the use of the Halbach array reduces the magnetic flux leakage and increases the amplitude of the harmonic components, and the specific magnetization angle is selected to improve the electromagnetic performance.

II. MOTOR TOPOLOGY AND OPERATING PRINCIPLE

A. MOTOR TOPOLOGY

The proposed DRCPVM has two rotors and a shared stator. And DRCPVM has different work modes because of having independent armature windings on both sides of the stator. Meanwhile, the model is divided into inner and outer parts to facilitate the following description.

For the outer part of DRCPVM, the pole pair number of PMs and winding is 44 and 4 respectively, and the number of stator outer teeth is 48. While the pole pair number of PMs and winding is 22 and 2 in the inner part, respectively. And the number of stator inner teeth is 24. The stator can be regarded as a complete structure with stator slots on both sides. The non-magnetic barrier is integrated into the stator for magnetic isolation. Two kinds of models are given in Fig. 1. Here, the DRCPVM is called Model I and the DRCPVM-HA is called Model II.

B. OPERATING PRINCIPLE

The proposed models are based on the principle of magnetic field modulation. The magnetomotive force formed by the three-phase windings can be calculated as follows [22]:

$$F_p = F_0 \sum_a \left[\frac{1}{6a+1} \lambda(a) \cos\left(\omega t - (6a+1) N_w \theta\right) \right] \quad (1)$$

$$F_0 = \frac{6\sqrt{2}\, NI}{\pi N_w} \quad (2)$$

$$\lambda(a) = \sin\left(\frac{6a+1}{2}\pi\right) \sin\left(\frac{6a+1}{6}\right) \quad (3)$$

where N is the coil turns number per phase, I is the RMS value of current in the coils, N_w is the pole pairs number of rotating magnetic field, θ is the mechanical angle and ω is angular velocity.

The permeance function of stator teeth is given by:

$$\Lambda = \Lambda_0 + \sum_{j=1,2,3\ldots}^{\infty} \Lambda_j \cos(j N_s \theta) \quad (4)$$

where Λ_j is the permeance amplitude due to jth harmonic, N_s is the number of stator teeth.

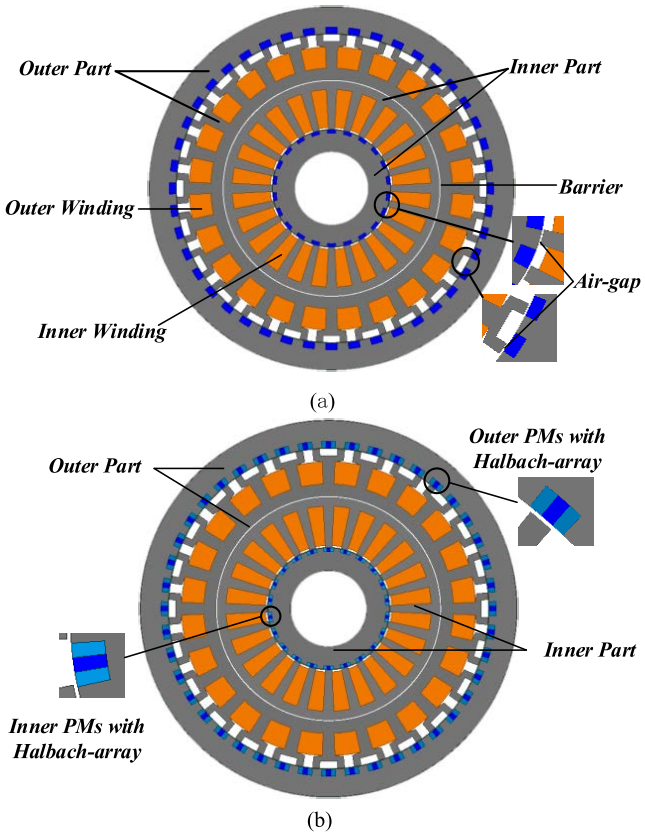

FIGURE 1. Topologies of the proposed models. (a) Model I: DRCPVM. (b) Model II: DRCPVM with the Halbach array (DRCPVM-HA).

The radial flux density of the vernier motor can be calculated as in the following equation:

$$\begin{aligned} &B_g(r,\theta) \\ &= F_p\Lambda \\ &= \Lambda_0 F_0 \sum_m \left[\frac{1}{6a+1}\lambda(a)\cos\left(\omega t-(6a+1)N_w\theta\right)\right] \\ &\quad+\frac{1}{2}F_0\sum_m\sum_j \frac{1}{6a+1}\lambda(a)\Lambda_j\cos\left[C_1\left(\theta-\frac{\omega t}{A_1}\right)\right] \\ &\quad+\frac{1}{2}F_0\sum_m\sum_j \frac{1}{6a+1}\lambda(a)\Lambda_j\cos\left[C_2\left(\theta-\frac{\omega t}{A_2}\right)\right] \end{aligned} \tag{5}$$

where C_1 and C_2 are expanded as follows:

$$\begin{aligned} C_1 &= -(6a+1)N_w + jN_s \\ C_2 &= -(6a+1)N_w - jN_s \end{aligned} \tag{6}$$

Moreover, the relation among the number of winding pole pairs, the number of stator teeth, and the orders of harmonics order are expressed as follows:

$$P_{a,b} = |-(6a+1)\cdot N_w + b\cdot N_s| \tag{7}$$

where $P_{a,b}$ is the order of harmonics order generated by modulation, a and b are integers, respectively.

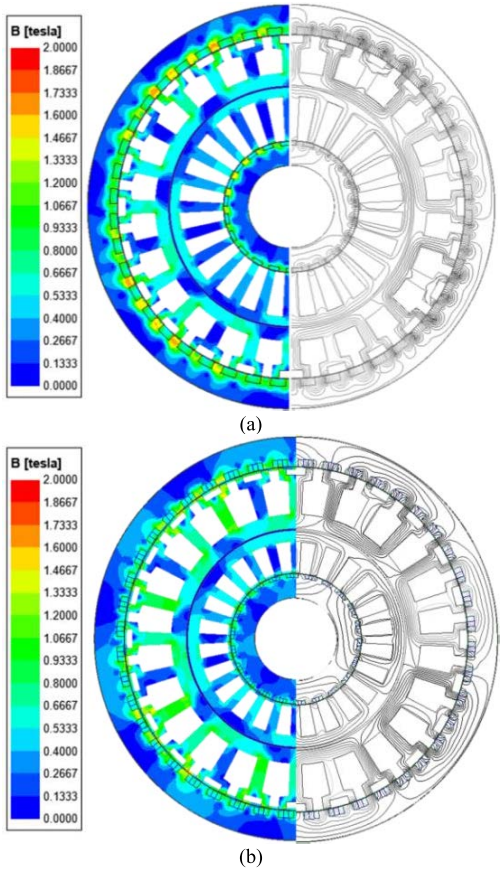

FIGURE 2. The magnetic field distributions of the motors. (a): Model I. (b): Model II.

Besides, the pole pair number of PMs, the number of stator teeth, and the pole pair number of rotating magnetic fields also satisfy the following equation:

$$N_p = N_s - N_w \tag{8}$$

where N_p is the pole pair number of PMs.

The gear ratio G_r is

$$G_r = -\frac{N_p}{N_w} \tag{9}$$

The magnetic field produced by the winding is opposite to the direction of the rotor rotation, so there is a '−' in (9).

In the traditional N-S structure, N and S poles are a pair of poles. But in the proposed consequent-pole structure, its N or S pole forms a pair of poles with the adjacent rotor iron boot.

The pole pair number of the inner PMs is 22 and that of the outer PMs is 44 in the proposed motor. And the consumption of PMs has a corresponding increase because the pole pairs number of PMs is large. By introducing the consequent-pole structure, the PMs remain the original pole pairs number, but the amount of PMs is reduced by half.

Under the no-load condition, the magnetic field distribution of the two models is shown in Fig. 2. The magnetic flux flows through the rotor, air gap, and stator to form the main magnetic circuit. Due to the different pole pair numbers of

the inner and outer windings, the loop number of the main magnetic circuit of the two parts is also different.

For the saturation phenomena in the two models, Model I is more saturated than Model II. In the rotor part of the two models, the magnetic leakage phenomena at the PMs of Model II are reduced compared with that of Model I. Due to the consequent-pole structure, Model I has the magnetic flux leakage phenomenon, and closed magnetic circuits are prone to appear at the PMs. While the magnetic flux leakage in Model II is reduced. Halbach array which uses the PMs with a specific magnetization angle can improve the main magnetic circuit and reduce the magnetic flux leakage in the consequent-pole structure.

III. OPTIMAL DESIGN

Regard Model I as the basic model, and the optimization are carried out. The optimization includes the size of the slots and the radian ratio of PMs. After Model I achieves the optimal structure, Model II introduces the Halbach array based on Model I. To obtain better electromagnetic performance in Model II, the magnetization angle of the Halbach array has been optimized. The following article is divided into three sections to optimize the motor.

A. SELECTION OF SLOT SIZE

Because of considering the size of the motor, the outer stator teeth adopt a slotted structure and the inner stator teeth have a non-slotted structure.

For the outer stator teeth, the size of slots has a large effect on the output torque of the outer rotor. For the inner stator teeth without slots, the size of the stator teeth has little effect on the performance of the motor, but the size of stator slots should be guaranteed to place a certain number of turns of windings. Based on the above description, this article has carried out a parameterized analysis of the size of the stator outer teeth.

The outer stator teeth is shown in Fig. 3. Referring to the center of the circle O, the width of the slot is defined as β. The height of the slot represents the vertical distance between the upper and lower sides of the slots in the horizontal direction, and slot height is defined as h. The definition of slot width and slot height has been finished, then the parametric analysis which includes both slot width and height will be carried out at the same time.

The variation of torque with different teeth slots parameters is shown in Fig. 4. And this shows that the slot width and height have an influence on the torque. To obtain the optimal slot parameters, the width and height of the slot are changed at the same time and the torque under the different parameters is recorded. Through simulation calculation, the torque achieves the maximum value when slot height h is 4 mm and slot width β is 6.5 °. The optimal point in Fig.4 represents the torque reaching the maximum value of 50.60 Nm.

B. RADIAN RATIO OF PERMANENT MAGNETS

The radian ratio of PMs also plays an important role in electromagnetic performance, and it is called K in this paper.

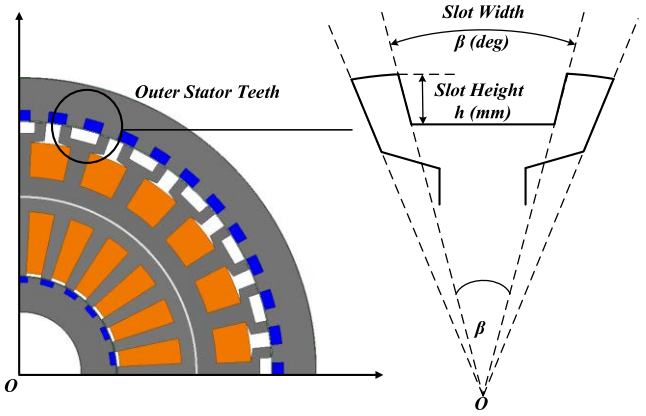

FIGURE 3. The structure of the outer stator teeth.

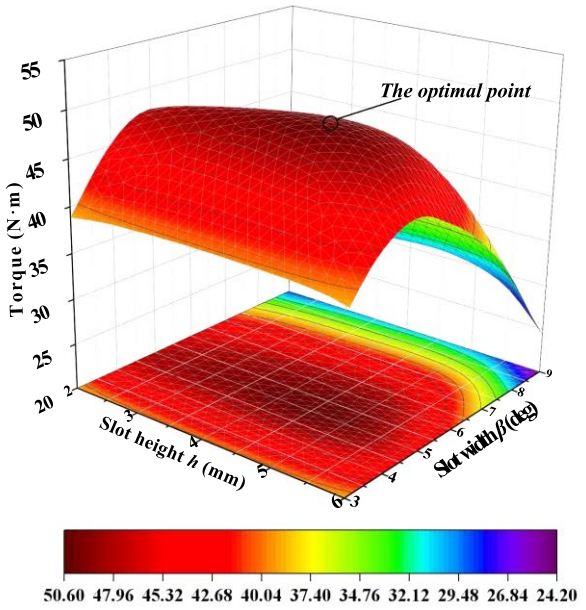

FIGURE 4. Outer rotor torque varies with the parameters of stator teeth slots.

The formula for K in traditional N-S pole structure is different from that consequent-pole structure.

In the traditional N-S pole structure, the formula for K is as follows:

$$K = \frac{\tau_{pm}}{\frac{2\pi}{2N_p}} = \frac{\tau_{pm} \cdot N_p}{\pi} \tag{10}$$

where K is the radian ratio of PMs, τ_{pm} is the radian occupied by PMs and N_p is the number of PMs pole pairs.

For the traditional N-S pole structure. To ensure the rationality of the structure, the value of K cannot be greater than 1. The arrangement of the PMs is shown in Fig. 5 when K is 1. At this time, the adjacent PMs are arranged on the rotor surface without gaps.

It is shown in Fig. 6 that the arrangement of PMs in the consequent-pole motor. The pole pair number of PMs in Fig. 5 and Fig. 6 are the same, but the amount of PMs in both structures is different. In the consequent-pole structure, the

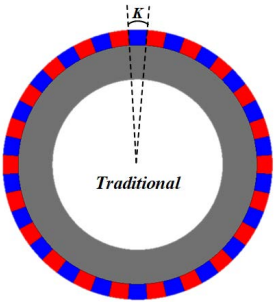

FIGURE 5. The radian ratio K in the traditional N-S pole structure.

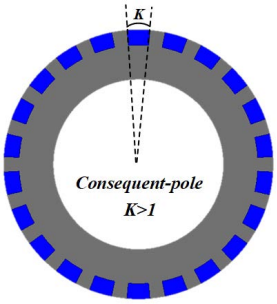

FIGURE 6. The radian ratio K in the consequent-pole structure.

radian occupied by a piece of PM could be larger than that in the traditional structure.

In the consequent-pole structure, the number of PMs has been reduced by half. So the formula for K is redefined as follows:

$$K = \frac{\tau_{pm}}{\frac{2\pi}{N_p}} = \frac{\tau_{pm} \cdot N_p}{2\pi} \tag{11}$$

That can be seen from the above two formulas, the difference between the two formulas is the coefficient in front of N_p. In consequent-pole structure, a pole pair of PMs has only a N or S pole, so the coefficient of N_p is 1. While the coefficient is 2 in the traditional structure. The value of K in the consequent pole could exceed 1 because of the coefficient. According to the above discussion about the coefficient, the K of the consequent-pole structure has a wider range of values than the K of the traditional structure.

The value range of K is set to find out the rule of torque changing with it. K_1 and K_2 are the radian ratio of PMs in the outer and inner rotors respectively.

The torque of outer and inner rotors changing with K is shown in Fig. 7. For the outer and inner rotors, the trend of torque changing with the K is firstly increasing and then decreasing. The torque of the outer rotor reaches the maximum when the K_1 is 1.2, and the torque is 54.36 Nm. For the inner rotor, the torque reaches the maximum when the K_2 is 1.2, and the torque is 16.48 Nm. The consequent-pole structure with $K = 1.2$ uses fewer PMs than the traditional structure with $K = 1$.

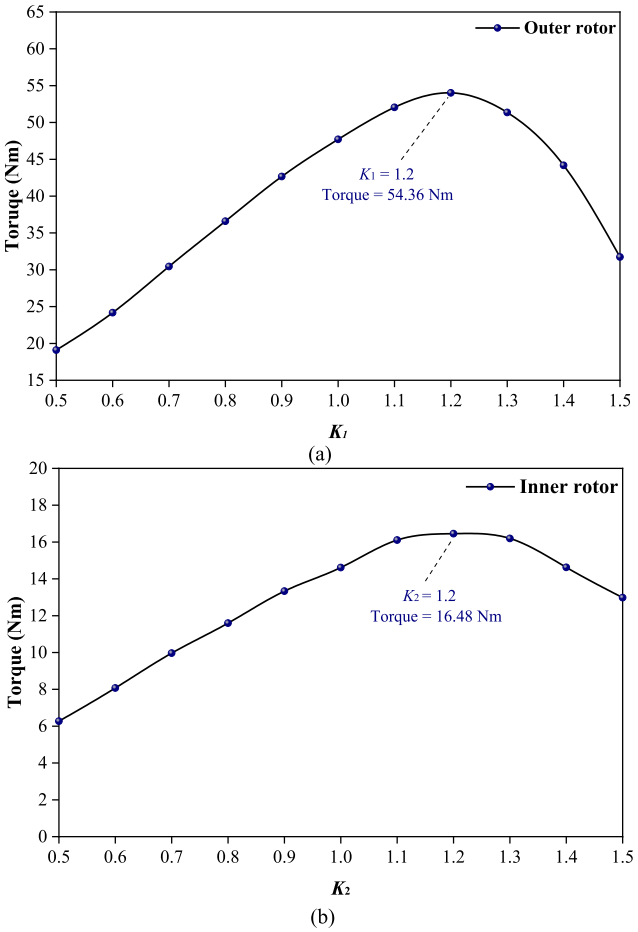

FIGURE 7. Torque under different values of K in the consequent-pole structure (a): The outer rotor. (b): The inner rotor.

The parameters of the proposed motor are changed to achieve optimal torque performance. The above optimization is based on the Model I. In the next section, on the basic Model I, Model II with Halbach array will be optimized.

C. HALBACH ARRAY WITH THE MAGNETIZATION ANGLE

Because the consequent-pole structure of Model I will cause magnetic flux leakage. To solve this problem, the Halbach array is introduced to establish Model II. In Model II, the PMs are divided into three pieces to form the Halbach array. The PMs in the middle piece remain in the original radial magnetization direction, but the PMs on both sides have a specific magnetization angle.

Model II is a dual rotor structure, there are PMs with Halbach array in both rotors. Although the magnetization directions of the Halbach array are different in these two rotors, the function of the Halbach array is to make more magnetic flux flow into the stator to form main magnetic circuits.

The PMs with Halbach array is given in Fig. 8, and the magnetization angle is defined as α. Because the magnetization directions of PMs on both sides of the Halbach array are symmetric, the '$-$' in front of α is to distinguish the magnetization directions on both sides. The following

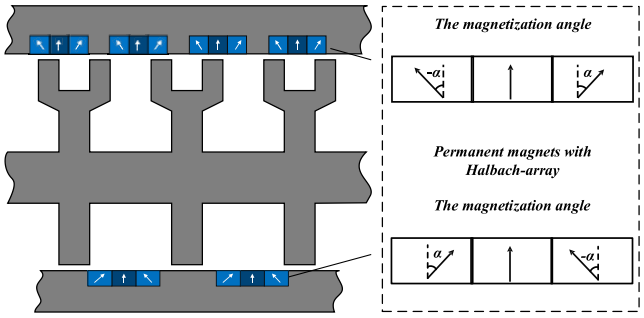

FIGURE 8. Permanent magnets with Halbach array of the outer and inner rotor.

description of α is to discuss its degree of angle, and the magnetization directions of the Halbach array are consistent with those shown in Fig. 8.

In the coordinate system shown in Fig. 9, take a magnet for the analysis of magnetization direction. The angle between $\alpha = 0$ and the magnetization vector is the magnetization angle. And in polar coordinates, the magnetization vector has radial and circumferential components which are related to the magnetization angle.

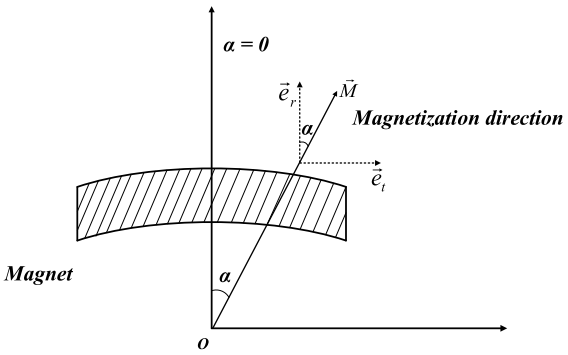

FIGURE 9. Magnetization direction and angle in polar coordinates.

The amplitude of magnetization M is calculated as the following equation [23]:

$$M = \frac{B_r}{\mu_0} \tag{12}$$

where μ_0 is the permeability in the air and B_r is the remanence of PMs.

In polar coordinates, the magnetization vector $\vec{M}$ is expressed by [24]:

$$\vec{M} = M_r\vec{e}_r + M_t\vec{e}_t = M\cos\alpha\vec{e}_r \mp M\sin\alpha\vec{e}_t \tag{13}$$

where $\vec{e}_r$ and $\vec{e}_t$ are the unit vector in the radial and circumferential directions, '−' is for the external field and '+' is for the internal field.

The Halbach array makes the field distribution concentrated on one side and dispersed on the other side, which is shown in Fig. 10. For the Halbach array in the outer rotor, it enhances the internal magnetic field. Meanwhile, the Halbach array in the inner rotor enhances the external field.

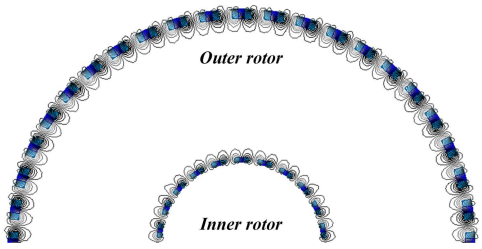

FIGURE 10. Magnetic field distribution of permanent magnets with Halbach array in the air.

TABLE 1. Results at different magnetization angles.

Magnetization angle (deg.)	Outer Back-EMF (V)	Inner Back-EMF (V)
0	115.30	37.13
15	131.54	41.68
30	143.17	42.98
45	146.30	43.62
60	144.40	41.29
75	135.54	37.88
90	120.94	33.05
105	101.49	27.15
120	78.79	20.45

In a dual rotor structure, the need for enhancing the magnetic field of internal and external air gaps is met by Halbach array.

Take the magnetization angle $\alpha = 0$ as a reference. To study the effect of the magnetization angle on the electromagnetic performance of the motor, the magnetization angle in the range of 0° to 120° will be sampled and analyzed. Referring to the radial upward direction, when the magnetization angle α is greater than 90°, the magnetization direction is no longer upward, and it will have a negative effect on the PM excitation magnetic circuit at the same time.

Every 15° is chosen as a measuring point. The outer and inner rotors are analyzed respectively. As the magnetization angle changes, the no-load back EMF and torque at each measuring angle are recorded.

When the magnetization angle is 0°, it means that the original radial magnetization direction of the PMs is not changed and the Halbach array has not produced any effect. Therefore, take the data recorded at 0° as a reference, and the simulation results at other measuring angles are compared with it to judge the effect of the magnetization angle. Table 1 shows that the no-load back-EMF of the outer rotor part and the inner rotor part increase first and then decrease with the change of the magnetization angle. The no-load back-EMF is less than the reference when the magnetization angle exceeds 90°. And when the magnetization angle is 45°, the amplitude of the outer and inner no-load back-EMF is the largest.

Fig. 11 shows that the no-load magnetic field distribution of Model II under different magnetization angles, and

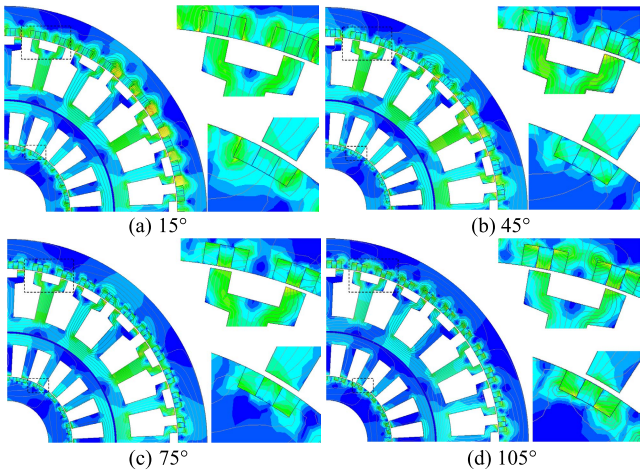

FIGURE 11. Magnetic field distributions at different magnetization angles.

different magnetization angles affect the path of flux lines. By comparing the no-load magnetic field distribution under the four magnetization angles, it is found that the degree of magnetic flux leakage at the PMs is lowest when the magnetization angle is 45°. There are fewer closed loops of magnetic flux lines near the PMs. Meanwhile, more magnetic flux lines flow into the side of stator teeth to form the main magnetic circuit. And the no-load back-EMF of Model II is the largest at this magnetization angle. When the magnetization angle exceeds 90°, it can be seen that the flux of the main magnetic circuits is reduced. And there is obvious flux leakage near the PMs, so the no-load back-EMF of the motor is decreased at these magnetization angles.

The trend of torque changing with the magnetization angle is shown in Fig. 12. The changing law of torque corresponds to that of no-load back-EMF. As the magnetization angle increases, the torque of the outer and inner rotor first increases and then decreases. When the magnetization angle is 45°, the torque of the outer and inner rotor reaches the maximum value of 68.72 Nm and 19.61 Nm respectively.

Based on the above research, it can be found that Model II has the best electromagnetic performance when the magnetization angle is 45°. Under this magnetization angle, the magnetic flux leakage of the motor is reduced and the main magnetic flux is improved. Therefore, the magnetization angle of 45° in the Halbach array is adopted.

IV. COMPARISON OF OPTIMAL PERFORMANCE

In Section III, the optimized Model I and Model II are established respectively.

These two models are consistent in motor structural parameters, but the difference is that Model II has used Halbach array. As shown in Table 2, the basic parameters of the proposed motors are given. Then, take the performance of Model I as a reference and compare it with Model II. Record the electromagnetic performance of two models under no-load and on-load conditions for comparative analysis.

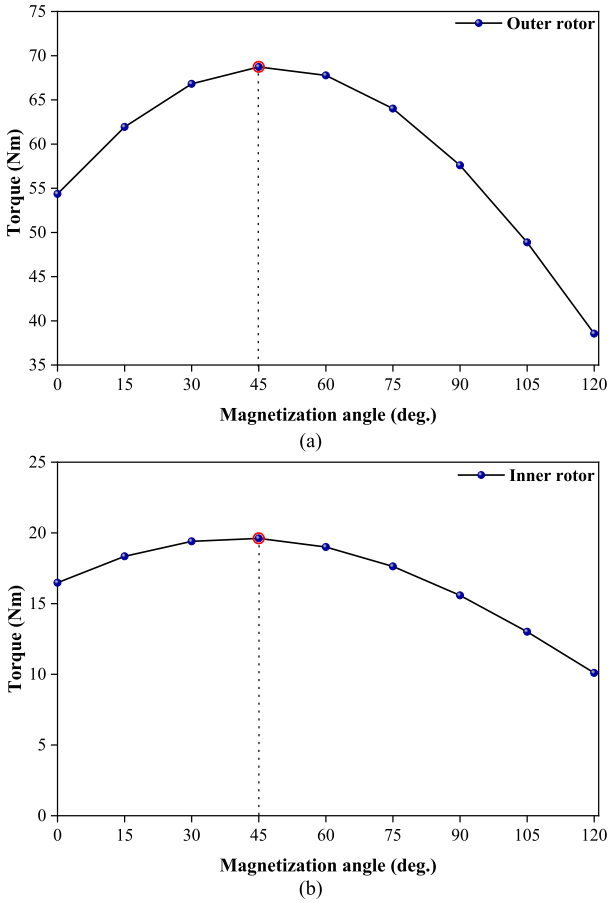

FIGURE 12. Output torque changes with different magnetization angles. (a): The outer rotor. (b): The inner rotor.

TABLE 2. Design data.

Parameters of the motors	Model I	Model II
Number of pole pairs of outer rotor PMs	44	44
Number of pole pairs of inner rotor PMs	22	22
Number of stator outside teeth	48	48
Number of stator inside teeth	24	24
Outer rotor outside radius (mm)	110	110
Inner rotor inside radius (mm)	22	22
Stator inside radius (mm)	35.5	35.5
Stator outside radius (mm)	93.4	93.4
Outer air-gap length (mm)	0.6	0.6
Inner air-gap length (mm)	0.5	0.5
Core axial length (mm)	60	60
Rated speed (rpm)	300	300
Magnetization angle (deg.)	0	45

A. NO-LOAD PERFORMANCE

Fig. 13 shows the flux density of the two models. Compared with Model I, Model II has an improvement in flux density.

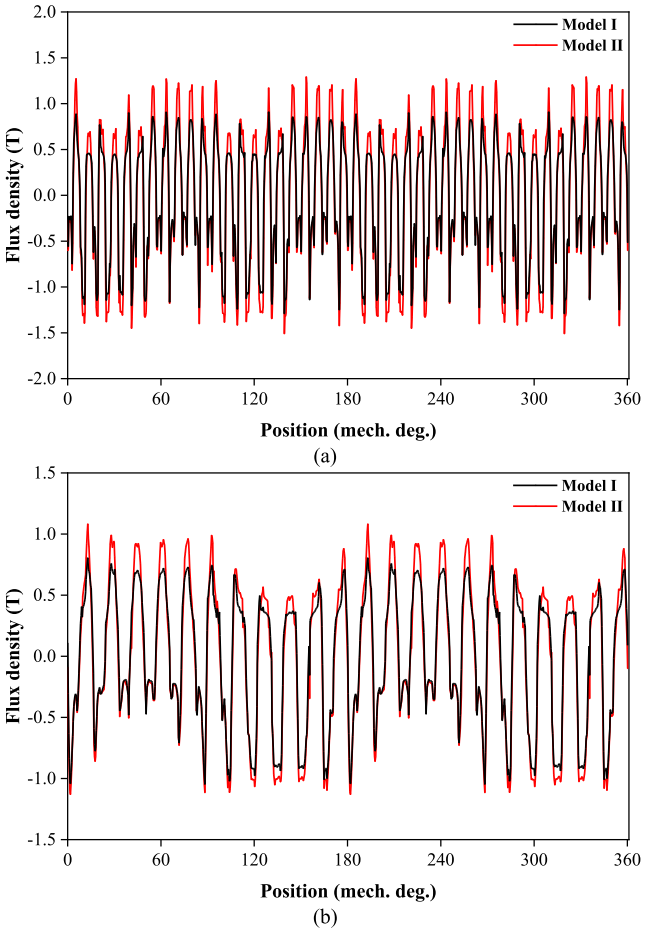

FIGURE 13. No-load flux density comparisons in air-gap. (a): Outer air-gap. (b): Inner air-gap.

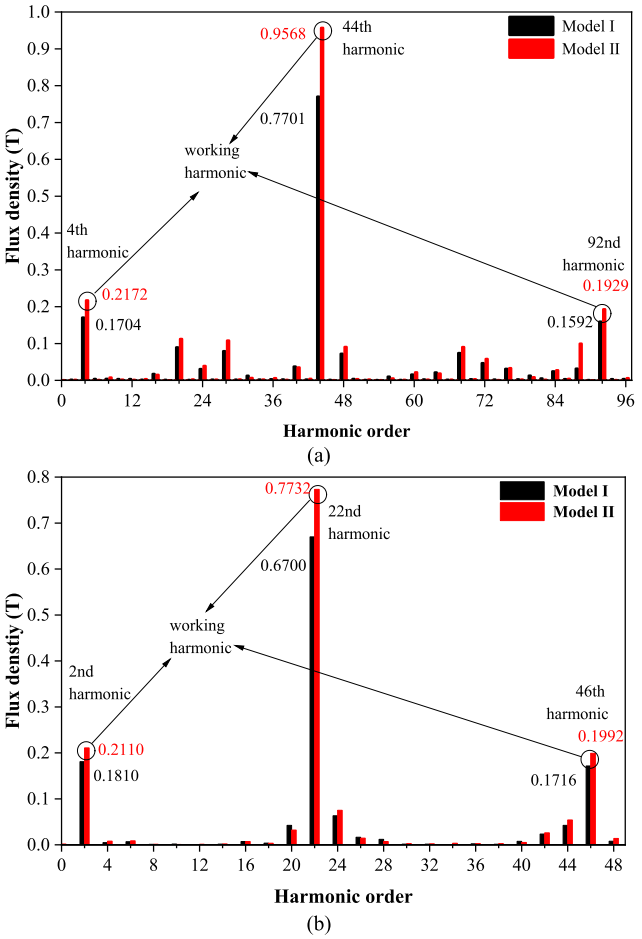

FIGURE 14. Harmonic decomposition comparisons of the air-gap flux density. (a): Outer air-gap. (b): Inner air-gap.

And this shows that the Halbach array with a magnetization angle of 45° could increase magnetic field intensity in the air gap, and also shows that the utilization of PMs has been improved.

Based on the working principle of the vernier motor, the outer air-gap main working harmonic orders are 4th, 44th, and 92nd, where the 44th harmonic occupies the largest component because the pole pair of outer rotor PMs is 44. Due to the pole pair number of outer and inner rotor PMs are not the same, both the air gaps in outer and inner parts have different working harmonic orders. The main working harmonic orders are 2nd, 22nd, and 46th in the inner air gap. Likewise, the pole pair number of PMs in the inner rotor is 22. And the 22nd working harmonic takes the largest amplitude.

As shown in Fig. 14 that the main working harmonic in outer air-gap, the amplitude of 4th, 44th, and 92nd harmonics are 0.2172, 0.9568, and 0.1929 respectively in Model II, and those of Model I are 0.1704, 0.7701, and 0.1592. Meanwhile, for the main working harmonic in inner air-gap, the amplitude of 2nd, 22th, and 46th harmonics are 0.2110, 0.7732, and 0.1992 respectively in Model II, and those of Model I are 0.1810, 0.670, and 0.1716. By comparing the main working harmonic amplitude of Model I and Model II, it can be further demonstrated that the Halbach array enhances the air-gap magnetic field of the motor.

The no-load back-EMF of the two models is shown in Fig. 15. For the no-load back-EMF amplitude of the outer rotor part, Model I is 115.30 V and Model II is 146.30 V. And For the no-load back-EMF amplitude of the inner rotor part, Model I is 37.13 V and Model II is 46.32 V.

B. ON-LOAD PERFORMANCE

For both outer and inner windings, when the three-phase windings are applied with the phase current of 10 A, the performance of torque in Model I and Model II can be seen in Fig. 16 and Table 3. In the outer rotor, the torque of Model I is 54.36 Nm and the torque ripple is 3.42%, while the torque of Model II is 68.72 Nm and the torque ripple is 1.69%. Compared with Model I, the outer rotor torque of Model II is increased by 26.42%. In the inner rotor, the torque of Model I is 16.48 Nm and the torque ripple is 0.71%, while the torque of Model II is 19.61 Nm and the torque ripple is 0.74%. Compared with Model I, the inner rotor torque of Model II is increased by 18.99%.

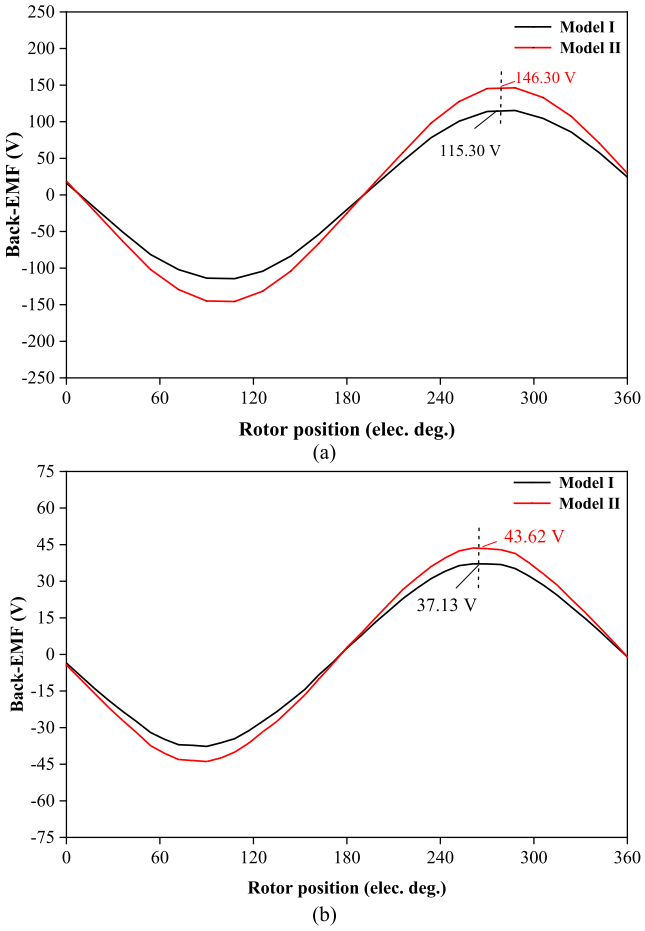

FIGURE 15. No-load back-EMF comparisons. (a): Outer rotor part. (b): Inner rotor part.

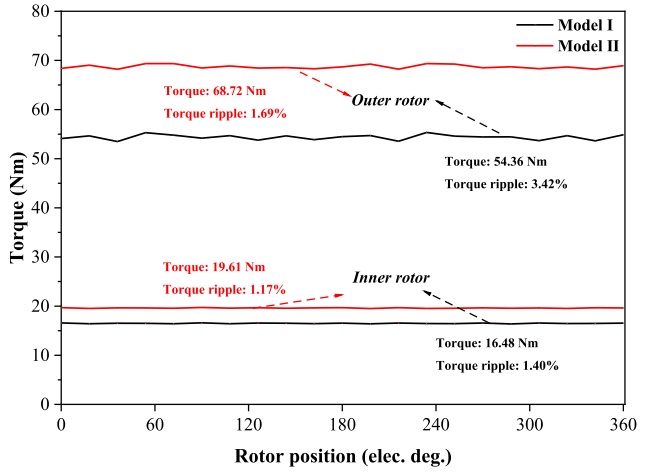

FIGURE 16. Output torque comparisons of the two models.

The formula for torque ripple can be expressed as follows:

$$T_{rip} = \frac{T_{\max} - T_{\min}}{T_{avg}} \times 100\% \tag{14}$$

where T_{max} is the maximum value of torque, T_{min} is the minimum value of torque, T_{avg} is the average value of torque and T_{rip} is the torque ripple.

TABLE 3. Torque of out rotor and inner rotor.

Item	T_{max} (Nm)	T_{min} (Nm)	T_{avg} (Nm)	T_{rip} (%)
Model I	55.34	53.48	54.36	3.42
	16.60	16.37	16.48	1.40
Model II	69.36	68.20	68.72	1.69
	19.73	19.50	19.61	1.17

TABLE 4. Volume and utilization rate of PMs.

Item	Location	The volume of PMs (cm3)	The utilization rate of PMs
Model I	Outer rotor	86.86	0.63
	Inner rotor	15.60	1.06
Model II	Outer rotor	86.86	0.79
	Inner rotor	15.60	1.26

The formula for PMs utilization is expressed as the following equation:

$$U_r = \frac{T_{avg}}{V_{pm}} \tag{15}$$

where V_{pm} is the volume of PMs and U_r is the PMs utilization rate.

It can be seen from Table 4 that Model II with the Halbach array increases the utilization rate of outer rotor PMs from 0.63 to 0.79 and increases the inner rotor from 1.06 to 1.26.

V. CONCLUSION

A DRCPVM-HA is proposed in this article. Two models have been established, one is DPCPVM which is regarded as a basic model, and another is DRCPVM-HA that the Halbach array is introduced on the basis of DRCPVM. The slot size of stator teeth and the radian ratio of PMs have an influence on electromagnetic performance, and the analysis of their parameters has been carried out. For DRCPVM-HA, the optimal magnetization angle is 45°, and the magnetic field distribution of the motor is improved at this angle. Meanwhile, the amplitude of working harmonics in the flux density of the outer and inner air gap is increased. For the maximum output torque of DPCPVM-HA, the outer rotor is 68.72 Nm and the inner rotor is 19.61 Nm. And the torque ripples of outer and inner rotors are 1.69% and 1.17% respectively. Compared with DRCPVM, the outer rotor torque of DRCPVM-HA has increased by 26.42%, and the inner rotor torque has increased by 18.99%. Under the condition of consuming the same volume of PMs, DPCPVM-HA has a higher utilization rate of the PMs. For the work modes, the torque of the outer rotor or inner rotor could be obtained simultaneously or separately according to the on-off state of two sets of windings.

REFERENCES

[1] Q. Hou, S. Ding, and X. Yu, "Composite super-twisting sliding mode control design for PMSM speed regulation problem based on a novel disturbance observer," *IEEE Trans. Energy Convers.*, vol. 36, no. 4, pp. 2591–2599, Dec. 2021.

[2] Q. Hou and S. Ding, "GPIO based super-twisting sliding mode control for PMSM," *IEEE Trans. Circuits Syst. II, Exp. Briefs*, vol. 68, no. 2, pp. 747–751, Feb. 2021.

[3] J. Li and K. T. Chau, "Performance and cost comparison of permanent-magnet Vernier machines," *IEEE Trans. Appl. Supercond.*, vol. 22, no. 3, Jun. 2012, Art, no. 5202304.

[4] C. Liu, J. Zhong, and K. T. Chau, "A novel flux-controllable Vernier permanent-magnet machine," *IEEE Trans. Magn.*, vol. 47, no. 10, pp. 4238–4241, Oct. 2011.

[5] H. Wang, S. H. Fang, H. yang, H. Y. Lin, D. Wang, Y. B. Li, and C. X. Jiu, "A novel consequent-pole hybrid excited Vernier machine," *IEEE Trans. Magn.*, vol. 53, no. 11, pp. 1–4, Nov. 2017.

[6] S. Niu, S. L. Ho, and W. N. Fu, "A novel direct-drive dual-structure permanent magnet machine," *IEEE Trans. Magn.*, vol. 46, no. 6, pp. 2036–2039, Jun. 2010.

[7] F. Yang, Y. Xie, and W. Cai, "The magnetic field analytical calculation in a novel double air-gaps permanent magnet Vernier synchronous motor," *IEEE Trans. Magn.*, vol. 57, no. 9, pp. 1–9, Sep. 2021.

[8] S. Niu, S. L. Ho, W. N. Fu, and L. L. Wang, "Quantitative comparison of novel Vernier permanent magnet machines," *IEEE Trans. Magn.*, vol. 46, no. 6, pp. 2032–2035, Jun. 2010.

[9] H.-Y. Li, Y. Liu, and Z. Q. Zhu, "Comparative study of air-gap field modulation in flux reversal and Vernier permanent magnet machines," *IEEE Trans. Magn.*, vol. 54, no. 11, pp. 1–6, Nov. 2018.

[10] T. Zou, D. Li, C. Chen, R. Qu, and D. Jiang, "A multiple working harmonic PM Vernier machine with enhanced flux-modulation effect," *IEEE Trans. Magn.*, vol. 54, no. 11, pp. 1–5, Nov. 2018.

[11] S. Niu, S. L. Ho, and W. N. Fu, "A novel stator and rotor dual PM Vernier motor with space vector pulse width modulation," *IEEE Trans. Magn.*, vol. 50, no. 2, pp. 805–808, Feb. 2014.

[12] D. K. Jang and J. H. Chang, "Design of a Vernier machine with PM on both sides of rotor and stator," *IEEE Trans. Magn.*, vol. 50, no. 2, pp. 877–880, Feb. 2014.

[13] S. L. Ho, S. Niu, and W. N. Fu, "Design and comparison of Vernier permanent magnet machines," *IEEE Trans. Magn.*, vol. 47, no. 10, pp. 3280–3283, Oct. 2011.

[14] X. Zhao, S. Niu, and W. Fu, "Torque component quantification and design guideline for dual permanent magnet Vernier machine," *IEEE Trans. Magn.*, vol. 55, no. 6, pp. 1–5, Jun. 2019.

[15] G. Liu, J. Yang, W. Zhao, J. Ji, Q. Chen, and W. Gong, "Design and analysis of a new fault-tolerant permanent-magnet Vernier machine for electric vehicles," *IEEE Trans. Magn.*, vol. 48, no. 11, pp. 4176–4179, Nov. 2012.

[16] L. Xu, G. Liu, W. Zhao, J. Ji, and X. Fan, "High-performance fault tolerant Halbach permanent magnet Vernier machines for safety-critical applications," *IEEE Trans. Magn.*, vol. 52, no. 7, pp. 1–4, Jul. 2016.

[17] K. Xie, D. Li, R. Qu, and Y. Gao, "A novel permanent magnet Vernier machine with Halbach array magnets in stator slot opening," *IEEE Trans. Magn.*, vol. 53, no. 6, pp. 1–5, Jun. 2017.

[18] D. Li, R. Qu, J. Li, and W. Xu, "Consequent-pole toroidal-winding outer-rotor Vernier permanent-magnet machines," *IEEE Trans. Ind. Appl.*, vol. 51, no. 6, pp. 4470–4481, Nov./Dec. 2015.

[19] N. Baloch, B.-I. Kwon, and Y. Gao, "Low-cost high-torque-density dual-stator consequent-pole permanent magnet Vernier machine," *IEEE Trans. Magn.*, vol. 54, no. 11, pp. 1–5, Nov. 2018.

[20] S.-U. Chung, J.-W. Kim, B.-C. Woo, D.-K. Hong, J.-Y. Lee, and D.-H. Koo, "A novel design of modular three-phase permanent magnet Vernier machine with consequent pole rotor," *IEEE Trans. Magn.*, vol. 47, no. 10, pp. 4215–4218, Oct. 2011.

[21] C. Shi, D. Li, R. Qu, H. Zhang, Y. Gao, and Y. Huo, "A novel linear permanent magnet Vernier machine with consequent-pole permanent magnets and Halbach permanent magnet arrays," *IEEE Trans. Magn.*, vol. 53, no. 11, pp. 1–4, Nov. 2017.

[22] K. Okada, N. Niguchi, and K. Hirata, "Analysis of a Vernier motor with concentrated windings," *IEEE Trans. Magn.*, vol. 49, no. 5, pp. 2241–2244, May 2013.

[23] Z. P. Xia, Z. Q. Zhu, and D. Howe, "Analytical magnetic field analysis of Halbach magnetized permanent-magnet machines," *IEEE Trans. Magn.*, vol. 40, no. 4, pp. 1864–1872, Jul. 2004.

[24] Z. Q. Zhu, Z. P. Xia, K. Atallah, G. W. Jewell, and D. Howe, "Novel permanent magnet machines using Halbach cylinders," in *Proc. 3rd Int. Power Electron. Motion Control Conf. (IPEMC)*, Beijing, China, vol. 2, Aug. 2000, pp. 903–908.

YING XIE (Senior Member, IEEE) received the Ph.D. degree in electric machine and apparatus from the Harbin Institute of Technology, Harbin, China, in 2008.

She worked as a Postdoctoral Researcher at the Huazhong University of Science and Technology, Wuhan, China, from 2010 to 2012. She worked as a Visiting Scholar at Sheffield University, U.K., in 2013. She is currently a Professor at the Harbin University of Science and Technology. Her current research interests include comprehensive physical fields calculation, including vibration characteristic and noise applied to electric motors, state monitoring and fault diagnosis of induction motors, and permanent magnet compound motor and drives for new energy electric vehicles.

SHOUCONG HE received the B.E. degree in electrical engineering and automation from the Jiangsu University of Science and Technology, Zhenjiang, China, in 2020. He is currently pursuing the M.E. degree in electric machine and apparatus with the Harbin University of Science and Technology, Harbin, China.

His current research interest includes permanent magnet Vernier motors design and analysis.

JIAWEI SHAO received the B.E. degree in electrical engineering and automation from the Harbin University of Science and Technology, Harbin, China, in 2020, where he is currently pursuing the M.E. degree in electric machine and apparatus. His current research interests include permanent magnet Vernier synchronous motors design and permanent magnet assisted synchronous reluctance motors design.

BITIAN YE received the B.E. degree in electrical engineering and automation from Henan Polytechnic University, Jiaozuo, China, in 2019. He is currently pursuing the Ph.D. degree in electric machine and apparatus with the Harbin University of Science and Technology, Harbin, China. His current research interests include variable flux memory motors design and high-power and high-speed permanent magnet motors design.

FAN YANG received the B.E. degree in electrical engineering and automation from Linyi University, Linyi, China, in 2016, and the M.E. degree in electrical engineering from Northeast Petroleum University, Daqing, China, in 2019. He is currently pursuing the Ph.D. degree in electric machine and apparatus with the Harbin University of Science and Technology. His current research interests include permanent magnet Vernier motors design and analytical calculation.

LIJING WANG received the B.E. degree in automation from Qiqihar University, Qiqihar, China, in 2012, and the M.S. degree in control science and engineering from the Department of Computer and Control Engineering, Qiqihar University, in 2016. She is currently pursuing the Ph.D. degree in electric machine and apparatus with the Harbin University of Science and Technology. Her current research interests include nonlinear control, motor control, pattern recognition, and intelligent systems.